Development of a Utility Negative Ion Test Equipment With RF Source at ASIPP

Jianglong Wei, Chundong Hu, Yahong Xie, Caichao Jiang, Lizhen Liang, Yan Wang, Yuming Gu, Jingyang Yan, Yongjian Xu, Yuanlai Xie, and NBI Team

***Abstract*— An RF-driven negative-ion source development program has been started at ASIPP-Hefei with a small test equipment, Hefei utility negative ion test equipment with RF source (HUNTER). It is devoted to some crucial issues of the RF-driven negative-ion source, such as the improvement of RF efficiency, the enhancement of the extracted negative-ion current density, and the promotion of the beam qualities. In the initial stage, the HUNTER negative-ion source conservatively adopted a similar structure of the ITER prototype source developed at IPP, Garching. It consists of single or double RF driver on the back side of a plasma expansion chamber, and a negative ion accelerator which is able to extract 120 beamlets up to 60 kV for 10 s. In the first phase operation of the HUNTER-ion source, a low-pressure (0.3 Pa) plasma has been successfully achieved by coupling 46-kW RF input power and different plasma parameters have been measured by using Langmuir probes and optical emission spectroscopy. Besides the negative-ion source, the HUNTER comprises the vacuum vessel, the special cooling system, the power supply system, and the source plasma and beam diagnostic system are also ready for the next phase operation of hydrogen negative ion beam extraction.**

***Index Terms*— Negative-ion source, neutral beam injection (NBI), RF-ion source.**

I. Introduction

IN ORDER to bridge the gap between ITER and fusion demonstration reactor and to realize the fusion power in China, a new fusion facility named the China Fusion Engineering Test Reactor (CFETR) is under conceptual design [1], [2]. Neutral beam injection (NBI) is one of the proposed external heating systems to bring the CFETR plasma to the ignition temperature. According to the latest physics design of CFETR [3], a steady-state neutral beam with the power higher than 20 MW at 0.8 MeV is demanded. At that high beam energy, the negative-ion-based NBI (N-NBI) system is inevitable to obtain an acceptable neutralization efficiency. While most of the NBI systems worldwide based on the positive ion sources, only facilities in Japan (JT-60 [4] and LHD [5], respectively) have N-NBI systems routinely in operation. Even for the upcoming ITER N-NBI system [6], [7], the required operational parameters are already very challenging. So that a full-scale test facility of ITER injector was launched to verify the overall design and to minimize the risks of unsuccessful operation [8], [9]. For a similar reason, a research project of the CFETR neutral beam test facility (NBTF) will be started in China for the next five years, as the most critical step toward the CFETR N-NBI system.

Considered the lack of research experience in the negative-ion source for NBI application in China, the **H**efei **U**tility **N**egative ion **T**est **E**quipment with **R**f source (HUNTER) has been set up in advance at the Institute of Plasma Physics, Chinese Academy of Sciences (ASIPP). The mission of HUNTER is to understand the characteristics of RF operation and negative ions generation and extraction, and to improve the RF efficiency and beam qualities. Although its beam energy is under 60 keV, the beamlets steering design for CFETR negative-ion source can be still verified and optimized beforehand on the HUNTER. Moreover, HUNTER is a flexible test equipment with kinds of diagnostic techniques. Thus, it can be used to test and compare exciting and new concepts.

As the reference for CFETR negative-ion source, the HUNTER target is to produce the hydrogen plasma for 3600 s and to extract the hydrogen negative ion beam of >350 A/m^2 for 10 s. The structure of HUNTER is shown in Fig. 1, which mainly comprises the negative-ion source, the vessel and auxiliary system, the power supply system, and the diagnostics system. The following sections of this paper describe the compositions of HUNTER in detail.

II. Negative-Ion Source

In the initial stage, a type of RF-driven negative-ion source with Cs seeding is conservatively adopted on the HUNTER. This type of ion source has been developed for demonstrating the ITER-required parameters at IPP, Garching, Germany, for twenty years [10]–[12]. As shown in Fig. 2, the HUNTER negative-ion source consists of one or two RF drivers with inductively coupled plasma (ICP) discharge, a plasma expansion chamber, and a negative-ion accelerator with three multi-aperture grids. The detailed design of HUNTER negative-ion source was described in [13].

Manuscript received June 22, 2017; revised October 15, 2017; accepted November 3, 2017. Date of publication January 24, 2018; date of current version May 8, 2018. This work was supported in part by the Key Program of Research and Development of Hefei Science Center, CAS, under Grant 2016HSC-KPRD002, in part by the National Natural Science Foundation of China under Grant 11405207, Grant 11505224, Grant 11505225, Grant 11575240, Grant 11675215, and Grant 11675216, and in part by the International Science and Technology Cooperation Program of China under Grant 2014DFG61950. The review of this paper was arranged by Senior Editor E. Surrey. *(Corresponding author: Jianglong Wei.)*

The authors are with the Institute of Plasma Physics, Chinese Academy of Sciences, Hefei 230031, China (e-mail: jlwei@ipp.ac.cn).

Color versions of one or more of the figures in this paper are available online at http://ieeexplore.ieee.org.

Digital Object Identifier 10.1109/TPS.2017.2771825

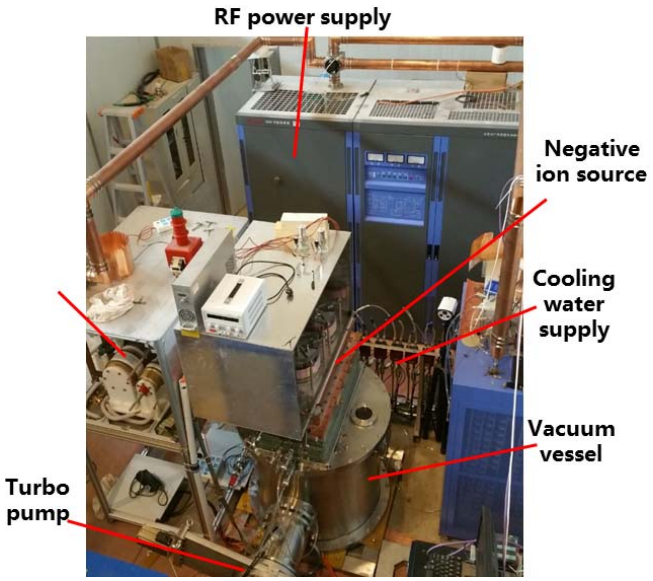

Fig. 1. Structure of HUNTER test equipment at ASIPP. The negative-ion source is installed with double RF drivers.

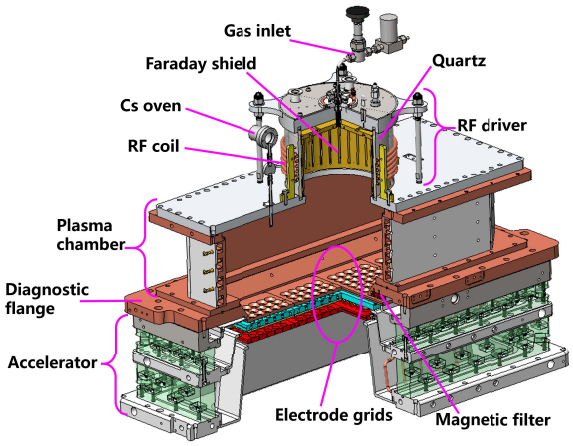

Fig. 2. 3-D diagram of HUNTER negative-ion source.

A. RF Driver

The driver is a cylinder including a lateral wall in quartz and a back cover in aluminum. The inner diameter of the quartz cylinder is 209 mm and the height is 120 mm. An RF coil with six windings is placed outside the quartz cylinder and connected to 1-MHz RF power supply (RF P.S.) and matching network. A copper-made Faraday shield with cooled water is inserted between the plasma and the quartz cylinder, to protect the quartz against the erosion and thermal radiation from the plasma.

As soon as the RF-ion source was available, the plasma production experiments were carried out extensively without extraction system [14], [15]. Two methods have been used to ignite the plasma. One was the start filament method. It could supply enough primary electrons for gas ionization, even for the required low-pressure gas. The other one was the pressure control method. A high-pressure gas was injected in an instant for plasma ignition. After an enough holding time (1–2 s), the gas pressure was decreased to a target value. As a result, the

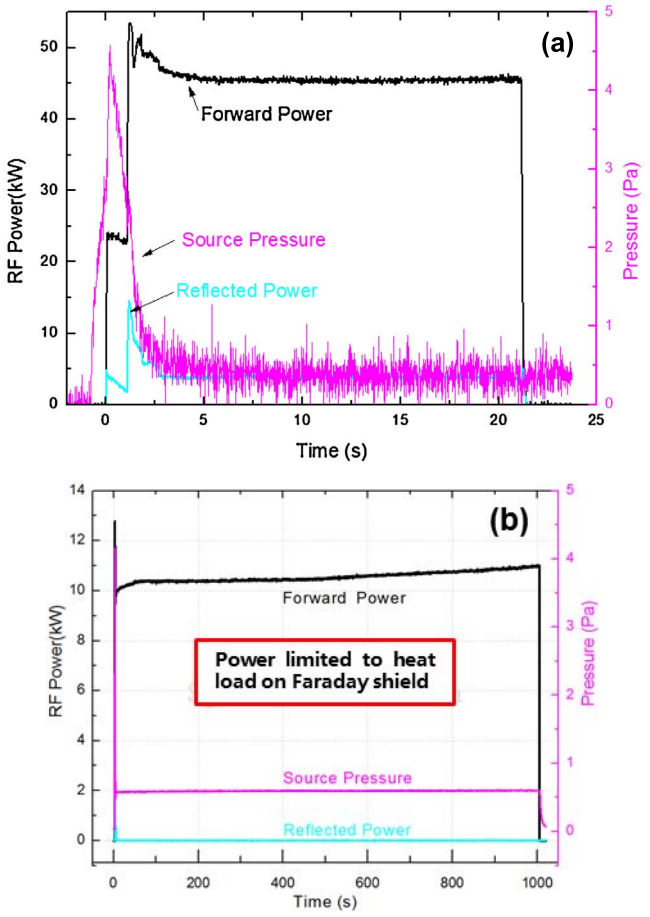

Fig. 3. Waveforms of plasma discharge in the RF driver. (a) Low-pressure and high-power RF plasma. (b) Long-pulse and low-power RF plasma.

stable high-power RF plasma discharge has been achieved. For example in Fig. 3(a), a shot of plasma discharge has lasted about 20 s with the RF input power of 46 kW and the source pressure was 0.3 Pa. However, the start filament method was more efficient and stable, thus which will be utilized more often in the future experiments.

Besides, the duration of RF plasma generation was attempted to extend up to 1000 s, as shown in Fig. 3(b). Through the water flow calorimetry, the heat load on the Faraday shield was measured to be around 50% of the RF input power. Although the coupled power was only 10 kW, the Faraday shield took 150 s to attain a thermal equilibrium state. It suggested that the current cooling design of the Faraday shield was not qualified for the long-pulse plasma discharge. Hence, a separated cooling scheme has been designed for the lateral wall and the back plate of the Faraday shield, respectively.

B. Plasma Chamber

The plasma chamber acts as an expansion region for the plasma mixture from multi-RF drivers. The plasma chamber is 65 cm in length, 26 cm in width, 19 cm in height, and made of copper. Compared with the former design, the height is shorter to reduce the Cs consumption due to the deposition on lateral walls. Four rows of magnets with an azimuthal configuration are installed around the chamber to form the

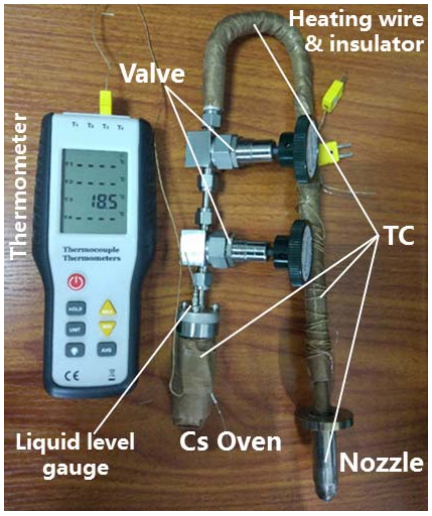

Fig. 4. Cs delivery system of HUNTER negative-ion source.

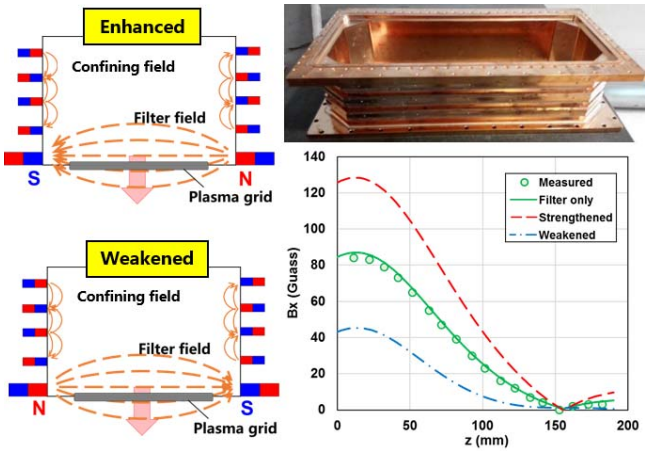

Fig. 5. Calculation results of the magnetic filter only (red solid line), enhanced (green dashed line) and weakened (blue dashed-dotted line) configurations, and the measured values of the magnetic filter only.

magnetic confining field. Its strength is about 1900 Gauss on the chamber wall.

The Cs vapor is delivered from an oven connected to the back plate of the plasma chamber. It can greatly increase the negative ions production from the Cs-covered surface with a low work function [16]–[18]. The Cs delivery system of HUNTER is shown in Fig. 4. The transmission pipe is winded with heating wire and is covered by thermal insulating tape. The temperature at Cs oven, transmission pipe, and nozzle are detected through four thermocouples. A feedback control of the temperature in oven and pipe is applied to change the Cs feeding rate.

The negative ions produced on the plasma grid (PG) surface are easily destroyed by the high-energy electrons [19], [20]. Therefore, an external magnetic filter is utilized on HUNTER negative-ion source to cool down the electron temperature through the filter field [21]. Two rows of filter magnets are embedded in opposite sides of the diagnostic flange (described in Section V-A). These magnets are made of Sm_2Co_{17}. Each filter magnet has a remanence of 1 T and a cross section of 10×40 mm^2. Considering the superposition with the confining field, there are indeed two kinds of filter field configurations. One is enhanced field configuration, where the bottom confining magnets have the same polarity direction with the filter magnets. The other one has a weakened field configuration. The field strength of magnetic filter only, enhanced and weakened configuration were calculated, respectively, along the centerline perpendicular to the diagnostic flange, as shown in Fig. 5. To benchmark the calculation results, the field strength of magnetic filter only was measured, which revealed a good agreement.

C. Negative Ion Accelerator

The HUNTER negative-ion source adopts a single-stage accelerator, which contains two insulators made by the fiber-enhanced epoxy resin, three grid supporting frames, and three electrode grids: PG, extraction grid (EG), and ground grid (GG). The aperture geometry of each grid is indicated

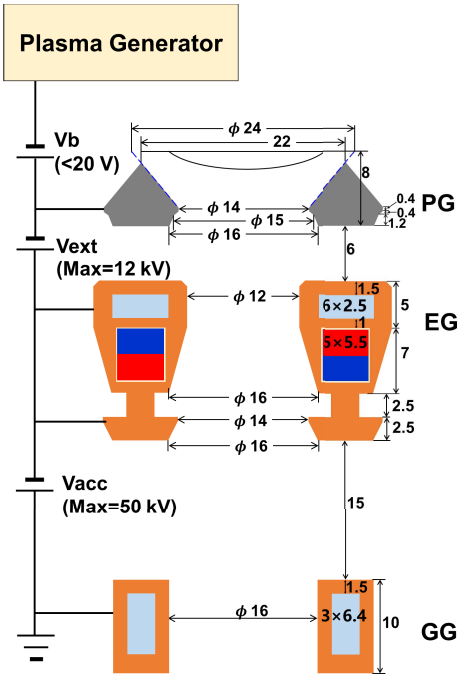

Fig. 6. Aperture geometry of actual grids of HUNTER negative-ion source. The light blue rectangles represent the cooling channels, and the red and dark blue rectangle combinations represent the EDMs. Their section sizes are indicated nearby. Distance unit is millimeter.

in Fig. 6. The extraction voltage between PG and EG is up to -12 kV and the maximum acceleration voltage between EG and GG is -50 kV. A special structure is attached on the EG for the electron trapping and the beam steering. All the grids are divided into four segments. Each segment has 6×5 apertures and the aperture spacing is 20 and 22 mm, respectively. Rows of electron deflection magnets (EDMs) are embedded inside the EG. Each EDM has a remanence of 1.05 T and a cross section of 5.5×5 mm^2.

The PG is positively biased against the plasma chamber and the bias voltage is close to the plasma potential. So that the PG works like a plane probe, which has collected nearly saturated electrons. The reduction of electron density in

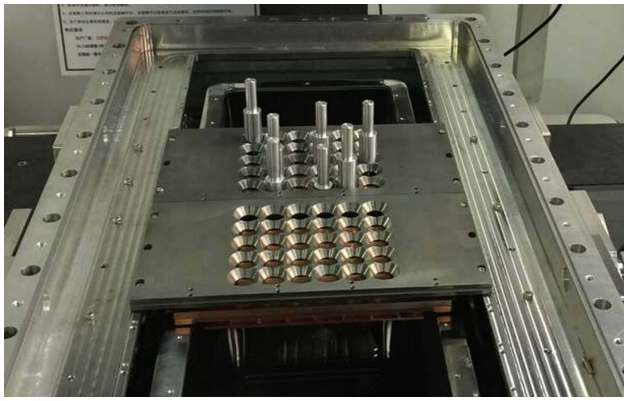

Fig. 7. Trial assembly for the grids on the optical coordinate measuring machine.

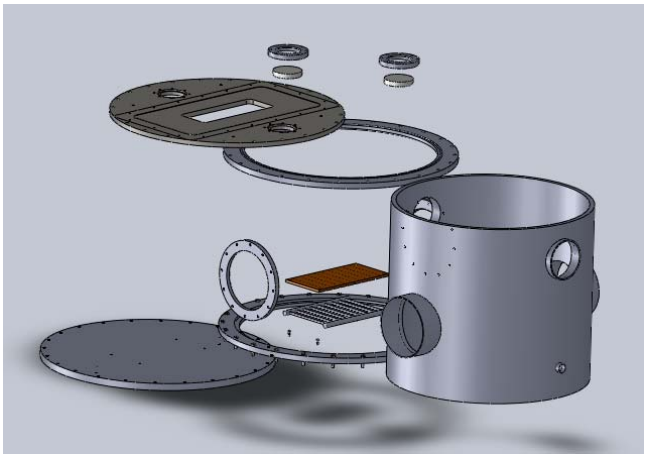

Fig. 8. 3-D explored view of HUNTER vacuum vessel.

front of the PG causes a suppression of the co-extracted electrons [22]–[24].

The single- and multibeamlet optics have been reviewed for the shape of grid aperture, in terms of beam divergence, beam deflection, and beam clearance [25]. The simulation results showed that the magnetic field of EDMs could effectively deflect the co-extracted electrons onto the top surface of EG and the impacting positions were mainly between two adjacent apertures. While this magnetic field also acted on the accelerated negative ions, even worse, the action distance of the magnetic force was unequal between the EDM upstream and downstream. As a result, a deflection angle was finally formed on one beamlet. Besides, the multibeamlets were electrically repulsed to each other. The cancelation or deterioration of the deflection effect and repulsion effect made the final emitting direction and angle different among each beamlet.

The manufacturing of those multichannel grid segments was based on the vacuum brazing technique [26]. There were several changes in the actual grids compared to the original design. The PG was made of the molybdenum instead of the copper. The two separated cooling channels between the EG apertures were merged into one large channel, to increase the reliability of vacuum brazing. The assembly and alignment of the grids were carried out on an optical coordinate measuring machine. A trial assembly is shown in Fig. 7.

III. Vacuum Vessel and Auxiliary System

Considered the flexibility and operability, a vertical cylinder has been set up as the HUNTER vacuum vessel, as shown in Fig. 8. It is 800 mm in diameter, 800 mm in height, and made out of stainless steel. The top plate is used for the installation of the ion source with a large opening and two viewing ports are reserved for spectroscopic diagnostics. On the lateral wall, two medium-sized ports are applied to transfer the cooling pipes and electric wires between vacuum and atmosphere. Another two large size ports are connected to the pumping system. A small port is used for vacuum pressure measurement. Inside the vessel, a copper-made and water-cooled beam dump is mounted.

In the initial experiments stage, two turbo pumps (totally 6000-L/s H_2 pumping speed) are installed on the vacuum vessel, for the RF plasma generation and the negative ions extraction only. But for the experiments of the negative ions acceleration, a cryogenic pump is planned to be equipped (30 000-L/s H_2 pumping speed). Another option is to utilize the additional vessel of the EAST neutral beam test stand (NBTS). It has a larger vacuum vessel (1.8 m in diameter, 2.1 m in length) and larger pumping system [27].

The cooling system can realize different temperatures for different requirements. The temperature of the cooling water for the walls of the plasma chamber is around 40 °C. It is better to the Cs for recycling from the internal walls [28]. A hot air of 150 °C is supplied inside the PG through the embedded cooling channels, in order to optimize the Cs thickness on the PG to maximize the negative ions production. And the other components of the ion source and the beam dump are cooled by the room temperature water.

IV. Power Supply System

The detailed design of the HUNTER power supply system is described in [29]. It mainly contains the following.

1) RF P.S. and matching network for generating the plasma.

2) Extraction voltage power supply (EXT P.S.) for extracting the negative ions.

3) Bias voltage power supply for changing the plasma voltage to suppress the co-extracted electrons.

4) Acceleration voltage power supply (ACC P.S.) for accelerating the negative ions.

As the requirement of acceleration voltage is not so high for HUNTER, the ACC P.S. adopts the existing high voltage power supply of the EAST NBTS at ASIPP [30]. The EXT P.S. is an independent unit instead of a branch of acceleration power supply. The key parameters of the newly developed power supplies are listed in Table I.

The RF P.S. is based on solid-state design, which has been successfully served for the experiments of RF driver with the corresponding matching network. A major effort during these experiments was adjusting the matching network to suppress the reflected power. Note that for the next stage experiments of negative ions acceleration, an isolation transformer should be added in the matching network. The capacitor at the primary side of the isolation transformer will be replaced by

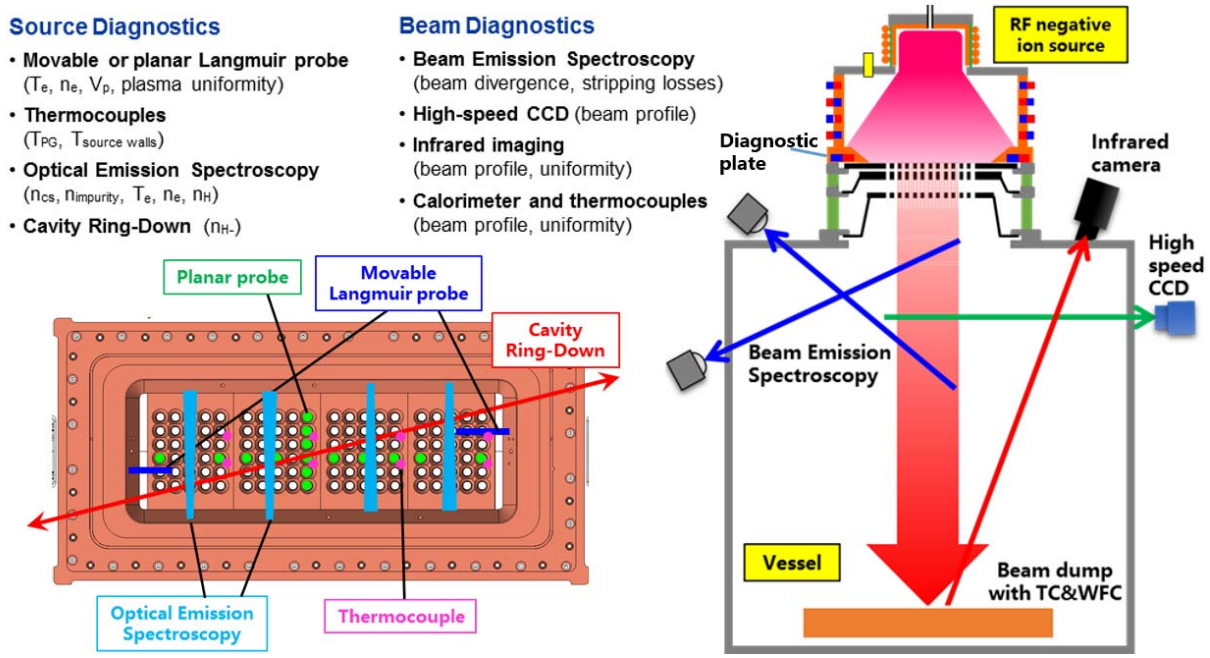

Fig. 9. Layout of HUNTER diagnostic system.

TABLE I
KEY PARAMETERS OF NEWLY DEVELOPED POWER SUPPLY

Power Supply	Parameters
RF P.S.	Solid state design Required output power 50 kW Maximum output power 60 kW RF frequency 1 MHz
Bias voltage P.S.	Rectifier design DC output 0-30V, 0-50A Alignment accuracy <1%
Extraction voltage P.S.	PSM design 19 modular of 800V/20A 8 modular of 100V/20A DC output 0-16 kV, 0-20A

a smaller one. Thus, the two capacitors in the matching network are both 2–4.3 nF. The EXT P.S. is based on pulse step module design, which has also passed the debugging tests. The control system of the EXT P.S. was developed. It consists of the cPCI computer for the fast real-time (∼ms) control, the monitor PC for the state inquiry of power supply, and the local controller inside each module.

V. DIAGNOSTIC SYSTEM

As a utility test equipment, HUNTER is equipped with kinds of diagnostic tools for source plasma and beam measurement.

A. Layout of HUNTER Diagnostic System

A copper-made plate is placed between the plasma chamber and the negative ion accelerator on the HUNTER negative-ion source. It is used as the diagnostic plate for measuring the plasma parameters in front of PG (i.e., extraction region). The bias voltage is applied between the diagnostic plate and the PG. The layout of the diagnostic plate is shown in the left side of Fig. 9. Two movable Langmuir probes are installed on the two ends. A cross-shaped array of planar probes is temporarily placed on the PG aperture, without the negative ions extraction. These two kinds of electrostatic probe can measure the electron temperature, the electron density, the plasma voltage, and the plasma uniformity. There are four lines of sight (LOS) for the optical emission spectroscopy (OES) on the diagnostic plate. On the back plate of the plasma chamber, there is another periscope-like LOS for OES. OES can measure the hydrogen atom density, the Cs density, the impurity density, and also the average electron density and temperature in a line [31]. Finally, a cavity ring-down (CRD) system can measure negative ion density [32], [33]. Several thermocouples are embedded inside the PG and attached on the source walls, to detect the temperature.

The layout of the beam diagnostics is also shown in the right side of Fig. 9. Two LOS for the beam emission spectroscopy can measure the beam divergence and the stripping losses by the Doppler shift spectroscopy [34], [35]. A high-speed CCD is applied to capture and analyze the picture of the beam profile. A special beam dump is designed and manufactured, as shown in Fig. 10. It is made of a copper back plate, with embedded cooling water circuit. An array of copper blocks is brazed on the beam-facing side. The copper block has a shape of a flat top pyramid. There is a small gap between any two adjacent blocks. Such designs can effectively reduce the lateral heat transfer. Thus, it is beneficial to the measurement of beam profile and uniformity by infrared imaging, for which an infrared camera is installed on the top plate of the vacuum vessel. Several thermocouples are installed from the back side and deep inside the blocks, so they can also measure the beam uniformity and profile. The beam dump also works as a calorimeter. The beam power is calculated by the temperature difference between inlet and outlet water.

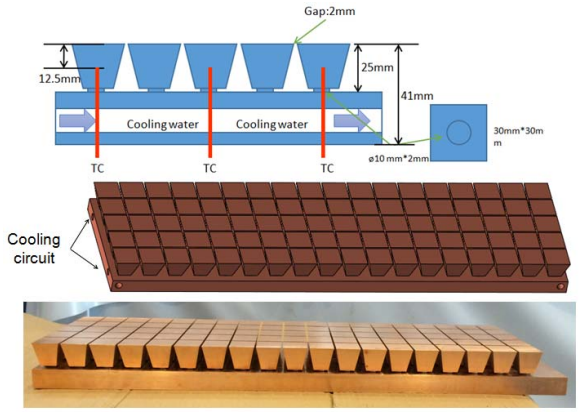

Fig. 10. Beam dump and also diagnostic calorimeter of HUNTER.

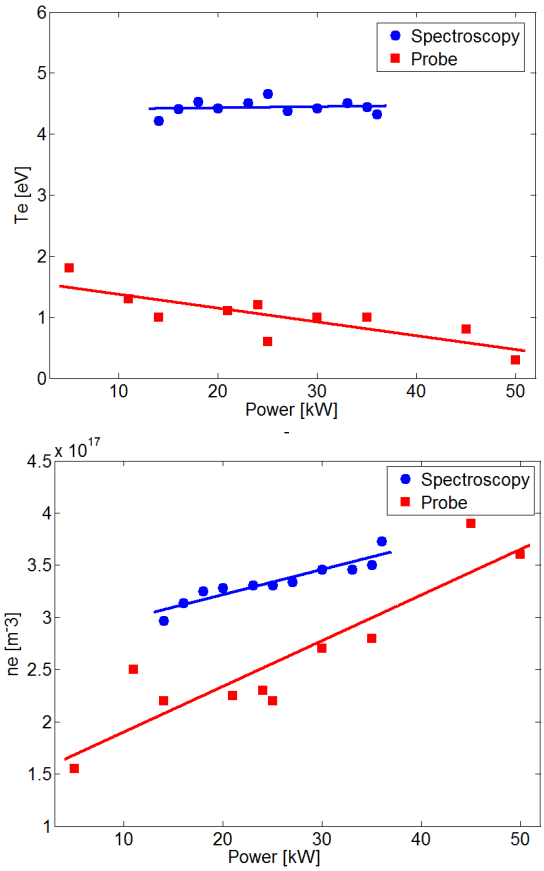

Fig. 11. Variation of the electron temperature and density with RF power measured by OES and Langmuir probe.

B. Preliminary Results of Source Diagnostics

During the experiments of the plasma generation in the RF driver, the OES and Langmuir probe have been already tested and served. Except for the commercial Langmuir probe, a self-developed double probe with *LC* filter (based on Band Rejection Filter design) was also applied, accompanying with a matching data acquisition and processing system. As mentioned earlier, a special OES system was installed on the back plate of the plasma chamber. A periscope-like structure was inserted into the chamber, to form the LOS at different depths.

The results of the electron temperature T_e and the electron density n_e measured by OES and Langmuir probe are shown in Fig. 11. The measuring LOS for the OES was at the top of the plasma chamber and the Langmuir probe was at the bottom. The source pressure was fixed at 0.5 Pa. Note that the accelerator was not equipped during the plasma generation experiments. So, the gas conductance and pressure drop were larger than normal condition. In the OES measurement, a little Xe and Ar gas (around 5% of the total gas injection quantity) were puffed into the RF driver as diagnostic gas. The emission spectrum of Xenon and Helium was used to calculate T_e and n_e based on the collisional–radiative (CR) model [36]. Obviously, the larger values of T_e and n_e measured by OES are reasonable, due to a closer measuring position to the RF driver.

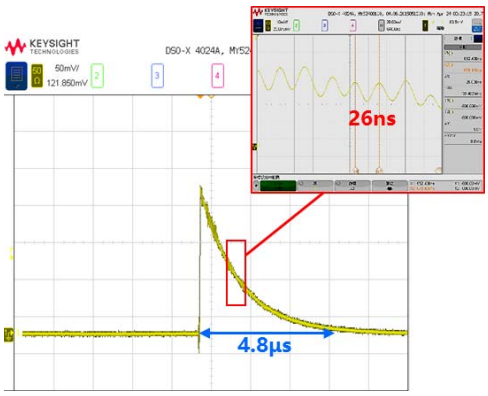

Fig. 12. CRD signal in a vacuum cavity of 1.2 m.

In order to test the CRD system in the desktop experiments, a vacuum cavity of 1.2 m, the laser light path, and the matching detection and analysis system were set up. A pulsed Nd: YAG laser is selected and the wavelength was 1064 nm. The reflectivity of the two mirrors was 99.999%. A photomultiplier tube was placed behind one mirror. The detection signal of the CRD in this cavity is shown in Fig. 12. The ring-down duration is 4.8 μs and the interval is 26 ns. According to the ring-down duration, the actual reflectivity of the mirror can be calculated in turn, that is 99.92%. The error is mostly from the transmission loss on the mirror.

VI. Conclusion

The requirement of CFETR NBI system is the beam energy of 0.8 MeV, the beam power larger than 20 MW, and the beam duration longer than 1 h. The HUNTER test equipment has been developed as a satellite of CFETR NBTF. The HUNTER negative-ion source, power supplies, vacuum vessel, and auxiliary system have been ready. Several diagnostic tools were developed for source plasma and beam measurement on HUNTER. Low-pressure and high-power RF plasma discharge has been achieved. The first experiments of negative ion extraction were carried out in July 2017.

References

[1] B. Wan, S. Ding, J. Qian, G. Li, B. Xiao, and G. Xu, "Physics design of CFETR: Determination of the device engineering parameters," *IEEE Trans. Plasma Sci.*, vol. 42, no. 3, pp. 495–502, Mar. 2014.

[2] Y. T. Song *et al.*, "Concept design of CFETR tokamak machine," *IEEE Trans. Plasma Sci.*, vol. 42, no. 3, pp. 503–509, Mar. 2014.

[3] Y. Wan *et al.*, "Overview of the present progress and activities on the CFETR," *Nucl. Fusion*, vol. 57, no. 10, p. 102009, Jun. 2017.
[4] Y. Takeiri *et al.*, "Development of intense hydrogen-negative-ion source for neutral beam injectors at NIFS," in *Proc. AIP Conf.*, Feb. 2013, vol. 1515. no. 1, pp. 139–148.
[5] A. Kojima *et al.*, "Achievement of 500 keV negative ion beam acceleration on JT-60U negative-ion-based neutral beam injector," *Nucl. Fusion*, vol. 51, no. 8, p. 083049, Aug. 2011.
[6] M. J. Singh *et al.*, "Heating neutral beams for ITER: Present status," *IEEE Trans. Plasma Sci.*, vol. 44, no. 9, pp. 1496–1505, Aug. 2016.
[7] R. S. Hemsworth *et al.*, "Overview of the design of the ITER heating neutral beam injectors," *New J. Phys.*, vol. 19, no. 2, p. 025005, Feb. 2017.
[8] V. Toigo *et al.*, "The PRIMA test facility: SPIDER and MITICA test-beds for ITER neutral beam injectors," *New J. Phys.*, vol. 19, no. 8, p. 085004, Aug. 2017.
[9] V. Toigo, "Progress in the realization of the PRIMA neutral beam test facility," *Nucl. Fusion*, vol. 55, no. 8, p. 083025, 2015.
[10] B. Heinemann *et al.*, "Towards large and powerful radio frequency driven negative ion sources for fusion," *New J. Phys.*, vol. 19, no. 1, p. 015001, Jan. 2017.
[11] U. Fantz *et al.*, "Physical performance analysis and progress of the development of the negative ion RF source for the ITER NBI system," *Nucl. Fusion*, vol. 49, no. 12, p. 125007, Nov. 2009.
[12] E. Speth *et al.*, "Overview of the RF source development programme at IPP Garching," *Nucl. Fusion*, vol. 46, no. 6, pp. S220–S238, May 2006.
[13] J. Wei *et al.*, "Design of the prototype negative ion source for neutral beam injector at ASIPP," *Plasma Sci. Technol.*, vol. 18, no. 9, pp. 954–959, Sep. 2016.
[14] Y. Xie *et al.*, "Development and preliminary results of radio frequency ion source," *Rev. Sci. Instrum.*, vol. 87, no. 2, p. 02B302, Feb. 2016.
[15] Y. Xie *et al.*, "Upgrade and experimental results of radio frequency ion source for neutral beam injector," *Fusion Eng. Des.*, vol. 114, pp. 72–75, Jan. 2017.
[16] M. Bacal and M. Wada, "Negative hydrogen ion production mechanisms," *Appl. Phys. Rev.*, vol. 2, no. 2, p. 021305, Jul. 2015.
[17] C. Wimmer, L. Schiesko, and U. Fantz, "Investigation of the boundary layer during the transition from volume to surface dominated H^- production at the BATMAN test facility," *Rev. Sci. Instrum.*, vol. 87, no. 2, p. 02B310, Feb. 2016.
[18] M. Yoshida *et al.*, "Time evolution of negative ion profile in a large cesiated negative ion source applicable to fusion reactors," *Rev. Sci. Instrum.*, vol. 87, no. 2, p. 02B144, Feb. 2016.
[19] Y. Takeiri, "Negative ion source development for fusion application (invited)," *Rev. Sci. Instrum.*, vol. 81, no. 2, p. 02B114, Feb. 2010.
[20] P. Franzen, L. Schiesko, M. Fröschle, D. Wünderlich, U. Fantz, and the NNBI Team, "Magnetic filter field dependence of the performance of the RF driven IPP prototype source for negative hydrogen ions," *Plasma Phys. Control. Fusion*, vol. 53, no. 11, p. 115006, Nov. 2011.
[21] J.-L. Wei *et al.*, "Conceptual design of magnetic filter for the prototype negative ion source at ASIPP," *Fusion Eng. Des.*, vol. 113, pp. 23–29, Dec. 2016.
[22] C. Wimmer, U. Fantz, and N. Team, "Extraction of negative charges from an ion source: Transition from an electron repelling to an electron attracting plasma close to the extraction surface," *J. Appl. Phys.*, vol. 120, no. 7, p. 073301, Aug. 2016.
[23] M. Bacal, M. Sasao, M. Wada, and R. McAdams, "Optimum plasma grid bias for a negative hydrogen ion source operation with Cs," *Rev. Sci. Instrum.*, vol. 87, no. 2, p. 02B132, Feb. 2016.
[24] M. Kisaki *et al.*, "Characteristics of plasma grid bias in large-scaled negative ion source," *Rev. Sci. Instrum.*, vol. 85, no. 2, p. 02B131, Feb. 2014.
[25] J.-L. Wei *et al.*, "Beam optics study of a negative ion source for neutral beam injection application at ASIPP," *Fusion Eng. Des.*, vol. 117, pp. 93–99, Apr. 2017.
[26] Y. Gu *et al.*, "Manufacturing and testing of multiaperture and multichannel grids for the prototype negative ion source for CFETR-NBI system," *Fusion Sci. Technol.*, vol. 72, no. 2, pp. 148–156, Aug. 2017.
[27] C. Hu *et al.*, "Overview of development status for EAST-NBI system," *Plasma Sci. Technol.*, vol. 17, no. 10, pp. 817–825, Oct. 2015.
[28] W. Kraus *et al.*, "Long pulse large area beam extraction with a RF driven H^-/D^- source," *Rev. Sci. Instrum.*, vol. 79, no. 2, p. 02C108, Feb. 2008.
[29] C. Jiang *et al.*, "Design of power supply system for the prototype RF-driven negative ion source for neutral beam injection application," *Fusion Eng. Des.*, vol. 117, pp. 100–106, Apr. 2017.
[30] Z. Liu, S. Liu, C. Jiang, Y. Xie, and C. Hu, *et al.*, "Design and development of a power supply system for NBI test stand of EAST," *J. Fusion Energ.*, vol. 33, no. 4, pp. 398–405, Jul. 2014.
[31] D. Wunderlich, U. Fantz, P. Franzen, R. Riedl, and F. Bonomo, "Optical emission spectroscopy at the large RF driven negative ion test facility ELISE: Instrumental setup and first results," *Rev. Sci. Instrum.*, vol. 84, no. 9, p. 093102, Sep. 2013.
[32] R. Pasqualotto, "Design of laser-aided diagnostics for the negative hydrogen ion source SPIDER," *J. Instrum.*, vol. 7, no. 4, p. C04016, Apr. 2012.
[33] H. Nakano *et al.*, "Cavity ringdown technique for negative-hydrogen-ion measurement in ion source for neutral beam injector," *J. Instrum.*, vol. 11, no. 3, p. C03018, Mar. 2016.
[34] R. Maurizio *et al.*, "Characterisation of the properties of a negative hydrogen ion beam by several beam diagnostic techniques," *Nucl. Fusion*, vol. 56, no. 6, p. 066012, Jun. 2016.
[35] L. Z. Liang *et al.*, "Preliminary experimental study of deuterium beam species for the EAST neutral beam injector by Doppler shift spectroscopy," *Phys. Scripta*, vol. 90, no. 4, p. 045603, Apr. 2015.
[36] X. M. Zhu, W.-C. Chen, J. Li, and Y.-K. Pu, "Determining the electron temperature and the electron density by a simple collisional–radiative model of argon and xenon in low-pressure discharges," *J. Phys. D, Appl. Phys.*, vol. 42, no. 2, p. 025203, Jan. 2009.

Authors' photographs and biographies not available at the time of publication.